AGU PUBLICATIONS

Geophysical Research Letters

RESEARCH LETTER
10.1002/2017GL075463

Key Points:
- Broadband recordings of *S*-*P* conversions allow for constraining compositional properties of deep Earth materials
- Stishovite is present in subducted eclogite and contributes to shear velocity softening
- Fragments of subducted oceanic crust are entrained in mantle flow and can be preserved at depths approaching 2,000 km

Supporting Information:
- Figure S1
- Supporting Information S1

Correspondence to:
S. M. Haugland,
samhaug@umich.edu

Citation:
Haugland, S. M., Ritsema, J., Kaneshima, S., & Thorne, M. S. (2017). Estimate of the rigidity of eclogite in the lower mantle from waveform modeling of broadband *S*-to-*P* wave conversions. *Geophysical Research Letters*, *44*. https://doi.org/10.1002/2017GL075463

Received 28 AUG 2017
Accepted 10 NOV 2017
Accepted article online 20 NOV 2017

Estimate of the Rigidity of Eclogite in the Lower Mantle From Waveform Modeling of Broadband *S*-to-*P* Wave Conversions

Samuel M. Haugland[1], Jeroen Ritsema[1], Satoshi Kaneshima[2], and Michael S. Thorne[3]

[1]Department of Earth and Environmental Sciences, University of Michigan, Ann Arbor, MI, USA, [2]Department of Earth and Planetary Sciences, Kyushu University, Fukuoka, Japan, [3]Department Geology and Geophysics, University of Utah, Salt Lake City, UT, USA

Abstract Broadband USArray recordings of the 21 July 2007 western Brazil earthquake (M_w=6.0; depth = 633 km) include high-amplitude signals about 40 s, 75 s, and 100 s after the *P* wave arrival. They are consistent with *S* wave to *P* wave conversions in the mantle beneath northwestern South America. The signal at 100 s, denoted as $S_{1750}P$, has the highest amplitude and is formed at 1,750 km depth based on slant-stacking and semblance analysis. Waveform modeling using axisymmetric, finite difference synthetics indicates that $S_{1750}P$ is generated by a 10 km thick heterogeneity, presumably a fragment of subducted mid-ocean ridge basalt in the lower mantle. The negative polarity of $S_{1750}P$ is a robust observation and constrains the shear velocity anomaly δV_S of the heterogeneity to be negative. The amplitude of $S_{1750}P$ indicates that δV_S is in the range from −1.6% to −12.4%. The large uncertainty in δV_S is due to the large variability in the recorded $S_{1750}P$ amplitude and simplifications in the modeling of $S_{1750}P$ waveforms. The lower end of our estimate for δV_S is consistent with ab initio calculations by Tsuchiya (2011), who estimated that δV_S of eclogite at lower mantle pressure is between 0 and −2% due to shear softening from the poststishovite phase transition.

1. Introduction

While seismic tomography has mapped the penetration of subducting lithosphere into the lower mantle on scales > 100 km (e.g., Fukao et al., 2001; Grand et al., 1997), array recordings of reflected or converted phases indicate that fine-scale (10–100 km) structure is present in the deep mantle (e.g., Kaneshima, 2016; Shearer, 2007). *S*-to-*P* conversions at depth *x*, denoted as S_xP, are excellent probes for detecting layering or localized heterogeneity in the lower mantle beneath deep-focus earthquakes. These shear wave conversions have been used to map small-scale seismic structure beneath the Marianas (e.g., Kaneshima & Helffrich, 1998), Tonga (e.g., Kaneshima, 2013; Li & Yuen, 2014; Yang & He, 2015), Indonesia (e.g., Kaneshima & Helffrich, 1994; Niu & Kawakatsu, 1997; Vanacore et al., 2006; Vinnik et al., 1998), South America (e.g., Castle & van der Hilst, 2003; Kaneshima & Helffrich, 2010), and northeast China (Niu, 2014). Kaneshima and Helffrich (1999) interpreted these small-scale, deep-mantle heterogeneities as fragments of subducted oceanic crust.

We inspected Transportable Array (TA) and Canadian National Seismic Network (CNSN) waveforms from 41 deep-focus (>300 km) earthquakes in South America since 2007. We detected high-amplitude S_xP conversions only in recordings of the 21 July 2007 M_w = 6.0 (latitude = 8.1°S; longitude = 71.3°W; depth = 633 km) western Brazil earthquake (the Brazil earthquake from hereon). The Brazil earthquake had a dip-slip source mechanism with optimal downward radiation of *SV*-polarized shear waves. The absence of clear *S*-*P* conversions in waveform data from other events is likely due to the unique focal mechanism of the Brazil earthquake.

Previous studies have modeled the amplitude and polarity of S_xP conversions (e.g., Kaneshima & Helffrich, 1999; Niu, 2014; Vinnik et al., 1998). In this paper we analyze broadband regional network waveforms by 2-D finite difference modeling at periods longer than 2 s. The broadband recording of $S_{1750}P$ at stations from the TA and CNSN elucidates the signal polarity and amplitude. By forward waveform modeling, we put constraints on the thickness and the shear velocity of the anomalous structure in the deep mantle responsible for generating $S_{1750}P$.

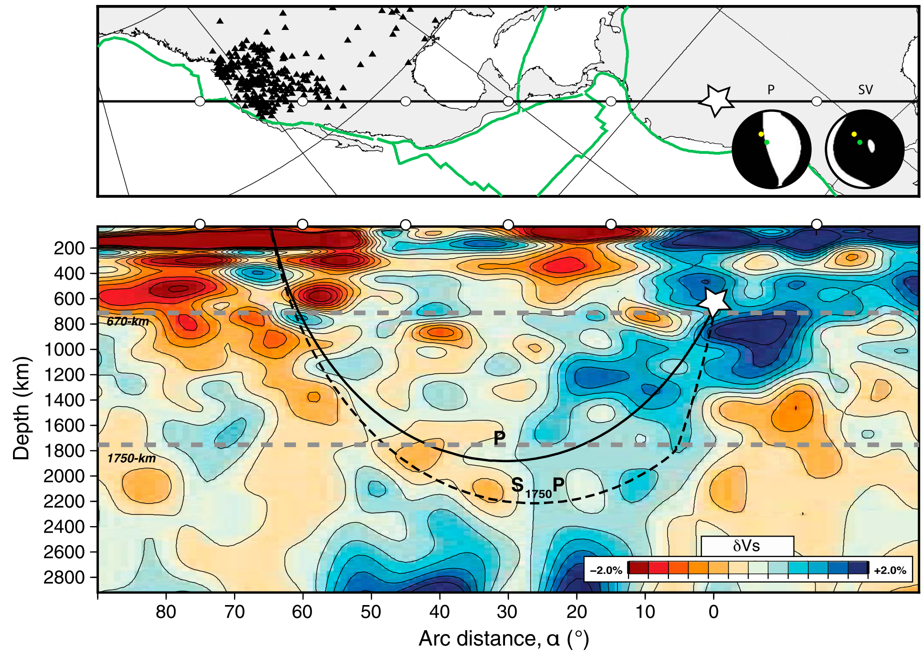

Figure 1. (top) Source-receiver geometry of the 10 July 2007 western Brazil earthquake. The star indicates the epicenter. The triangles indicate the locations of stations from the Transportable Array (TA) and the Canadian National Seismic Network (CNSN) used in the analysis. The black line is the great-circle arc through the Brazil event and the western U.S. The white circles on top are drawn every 15°. *P* wave and *SV* wave radiation patterns are shown on the lower right. Green circles on the radiation pattern indicate the $S_{1750}P$ takeoff direction. Yellow circles on *P* and *SV* radiation patterns indicate *P* and *S* wave takeoff directions, respectively. (bottom) Geometric raypaths of *P* (solid line) and $S_{1750}P$ (dashed line) for an epicentral distance of 65°. The raypaths are superposed on a NW-SE oriented cross section of the S40RTS model (Ritsema et al., 2011) through the Brazil event and the TA and CNSN stations. Note that $S_{1750}P$ is formed within a high-velocity anomaly in the lower mantle beneath South America.

2. S_xP Conversions in the Lower Mantle Beneath South America

2.1. Wave Geometry

S_xP is formed when the downward propagating *S* wave converts to a *P* wave at a discontinuity or heterogeneity in seismic velocity at depth *x* below the earthquake source. Beneath the Brazil earthquake, S_xP conversions form in a high-velocity structure that we interpret as the Nazca lithosphere subducted beneath western South America (Figure 1). We can distinguish S_xP from crustal reverberations and reflections off boundaries above the earthquake (i.e., $p_{410}P$ and $s_{410}P$) or beneath the receivers (e.g., $P_{410}s$ and $P_{660}s$) when its slowness can be determined using recordings from a wide-aperture network.

2.2. Waveforms From North America

More than 250 TA and CNSN stations in western North America recorded the Brazil earthquake between 56° and 73°. The record section of vertical component traces in Figure 2a shows the ground velocity after alignment on the *P* wave (at time 0). The seismic phases *PcP* and *pP* are reflections off the outer core and Earth's surface, respectively. Three S_xP signals at about 45 s, 75 s, and 100 s after the *P* arrival are visible throughout the section. The signals at 45 s, which may interfere with $p_{410}P$, and at 75 s are $S_{950}P$ and $S_{1250}P$, respectively. These conversions were formed about 3° off the great-circle path and have complex waveforms (see Figure S1 in the supporting information). We interpret the impulsive arrival at 100 s as $S_{1750}P$. Its arrival time decreases with increasing epicentral distance with respect to *P*, as expected for a S_xP conversion.

The vespagram in Figure 2b indicates that the slowness of $S_{1750}P$ is about 0.2 s per degree higher than predicted for a standard 1-D seismic model. This suggests that the $S_{1750}P$ conversion point is located farther from the earthquake hypocenter than expected for a 1-D wave speed model. Semblance is a measure of coherent energy in a stack of data arriving from a common conversion point. By semblance analysis, following

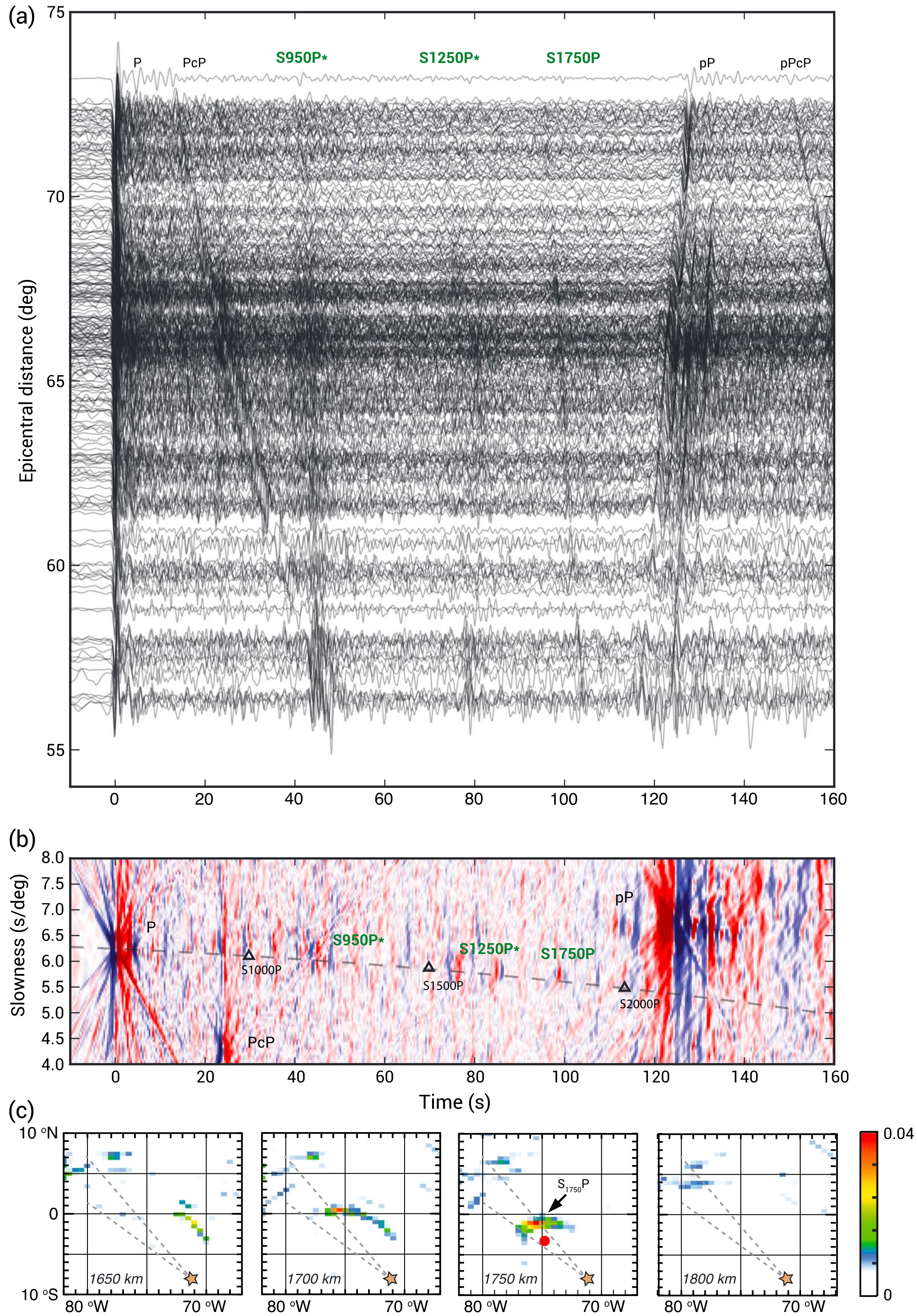

Figure 2. (a) Record section of velocity waveforms of the Brazil event aligned on the *P* wave arrival (at time 0). Labeled on top are the arrival times of the major phases *P*, *PcP*, *pP*, *pPcP*, and *S-P* conversions at 950 km, 1,250 km, and 1,750 km depth. The conversion depths of $S_{950}P$ and $S_{1250}P$ are shallower depths than expected for 1-D models because these phases propagate off azimuth for the Brazil earthquake (see Figure S1). (b) Vespagram of the absolute amplitude of the sum of waveforms as a function of time and signal slowness. The S_xP slowness branch is indicated by a dashed line. (c) Map view of semblance coefficients computed for a 0.5° × 0.5° × 50 km grid at 1,650 km, 1,700 km, 1,750 km, and 1,800 km depth. The warmest colors indicate where semblance values are the highest. The dashed lines represent the station azimuth range of the TA and CNSN stations with clear $S_{1750}P$ signals. The red circle at 1,750 km depth is the $S_{1750}P$ conversion point computed for a 1-D velocity structure.

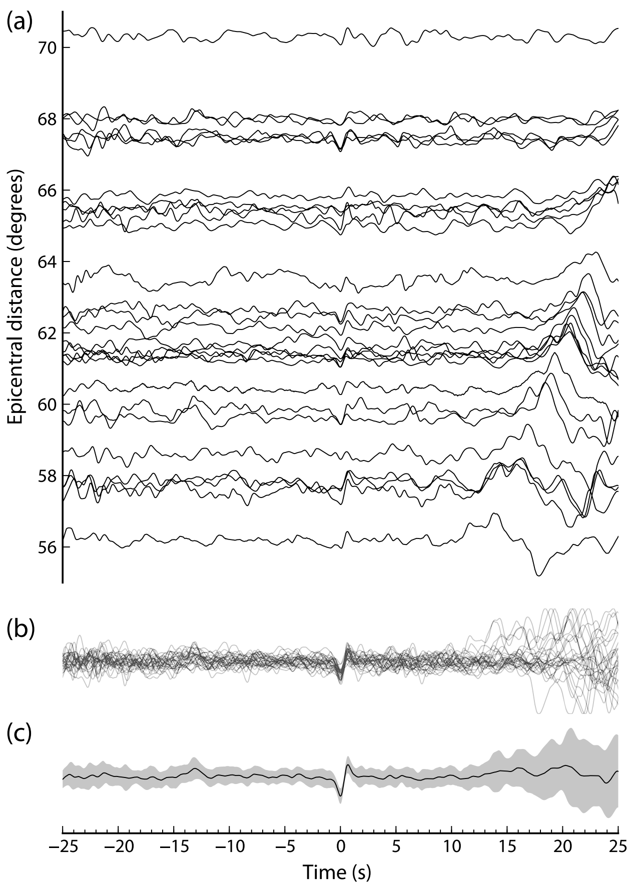

Figure 3. (a) Record section and (b) stacked displacement waveforms centered on $S_{1750}P$ from 30 TA and CNSN stations. The large-amplitude signal moving out with increasing distance is *pP*. (c) Sum of the displacement waveforms. The gray envelope is two standard deviations wide and indicates amplitude variability present in the data.

Kaneshima and Helffrich (2003), we locate the conversion point of $S_{1750}P$ between 1,700 and 1,750 km depth within the sector of source azimuths of the TA and CNSN stations but about 400 km to the NW of the 1-D predicted conversion location (Figure 2c). This is consistent with the $S_{1750}P$ slowness and traveltime observed in Figure 2b.

3. Waveform Modeling

The $S_{1750}P$ signal is recorded above noise level in 30 vertical displacement seismograms from the TA and CNSN. Figure 3 shows these waveforms and their sum after they have been aligned and scaled such that the *SV* wave, which converts into $S_{1750}P$, has an amplitude equal to 1. The $S_{1750}P$ signal in each of these 30 records is composed of a negative and a positive pulse separated by about 2 s, with varying amplitudes. The mean value of the peak-to-peak amplitude is 4.4% of the *SV* amplitude on the vertical component, and the two standard deviation of the amplitude is 3.4%.

Computed waveforms indicate that the waveform shape of $S_{1750}P$ is due to the interference of two *S*-to-*P* conversions at the upper and lower boundaries of a narrow velocity structure. These two conversions have opposite polarities. We model the heterogeneity that produces $S_{1750}P$ as a block centered on the ray-theoretical $S_{1750}P$ conversion point beneath the earthquake (Figure 4a). The block has a thickness h and makes an angle α with the equatorial plane.

We choose long blocks to avoid wave diffraction around them. We expect diffraction to reduce the amplitude of $S_{1750}P$, but it must be studied in 3-D. The *S* wave velocity contrast with respect to the ambient mantle is δV_S. Our synthetics indicate that anomalies in the *P* wave velocity and density do not affect the $S_{1750}P$ waveform significantly (see Figure S2).

We model the stack of the 30 high-amplitude $S_{1750}P$ waveforms using synthetics computed with the PSVaxi method (e.g., Thorne et al., 2013), a finite difference method similar to the SHaxi method developed by Jahnke et al. (2008). PSVaxi allows us to compute the full seismic wavefield of *P*-*SV* motions with the correct 3-D geometric spreading for a model of seismic structure in the plane of the great-circle arc. The 2-D grid of heterogeneity is expanded to 3-D spherical geometry by rotating it around the radial axis passing through the seismic source. Our PSVaxi synthetics include signals up to frequencies of 0.5 Hz (i.e., shortest dominant period of 2 s) but due to the assumed axisymmetry, signals from off-azimuth wave propagation or *SH*-to-*P* conversions cannot be modeled.

We compute synthetics for the PREM seismic model and for a 3-D model in which the block heterogeneity at 1,750 km depth is embedded within PREM. In the PREM model, we replace the 220 km, 400 km, and 670 km discontinuities by smooth gradients to suppress reflections and conversions produced in the upper mantle. We subtract the PREM and 3-D waveforms to isolate the $S_{1750}P$ signals.

Figures 4b and 4c compare the recorded $S_{1750}P$ signal (see Figure 3c) to synthetic waveforms for different block thicknesses h and shear velocity anomalies δV_S. The block thickness h controls the traveltimes of the entry and exit conversions and, therefore, the pulse width of $S_{1750}P$. The synthetics for $h = 2$ km and $h = 20$ km clearly underestimate and overestimate the recorded pulse width, respectively (Figure 4b). We find the best match for $h = 10$ km and use this value in our modeling. The shear velocity anomaly δV_S of the block determines the polarity of δV_S. A negative value for δV_S is required to reproduce the down-and-up swing of $S_{1750}P$ (Figure 4c).

Figure 5 compares the recorded peak-to-peak amplitude of $4.4 \pm 3.4\%$ to predicted amplitudes when varying δV_S (in Figure 5a) and block angle α (in Figure 5b). The amplitude of $S_{1750}P$ depends linearly on δV_S. A value of $\delta V_S = -7\%$ produces a match between the computed and recorded mean peak-to-peak amplitude of $S_{1750}P$, but values of δV_S between -1.6% and -12.4% match the amplitude within its uncertainty range. The amplitude of $S_{1750}P$ depends on α in a nonlinear manner. The predicted $S_{1750}P$ amplitude is highest when $\alpha \approx 10°$. Changing α by 20° decreases the $S_{1750}P$ amplitude by as much as 30%.

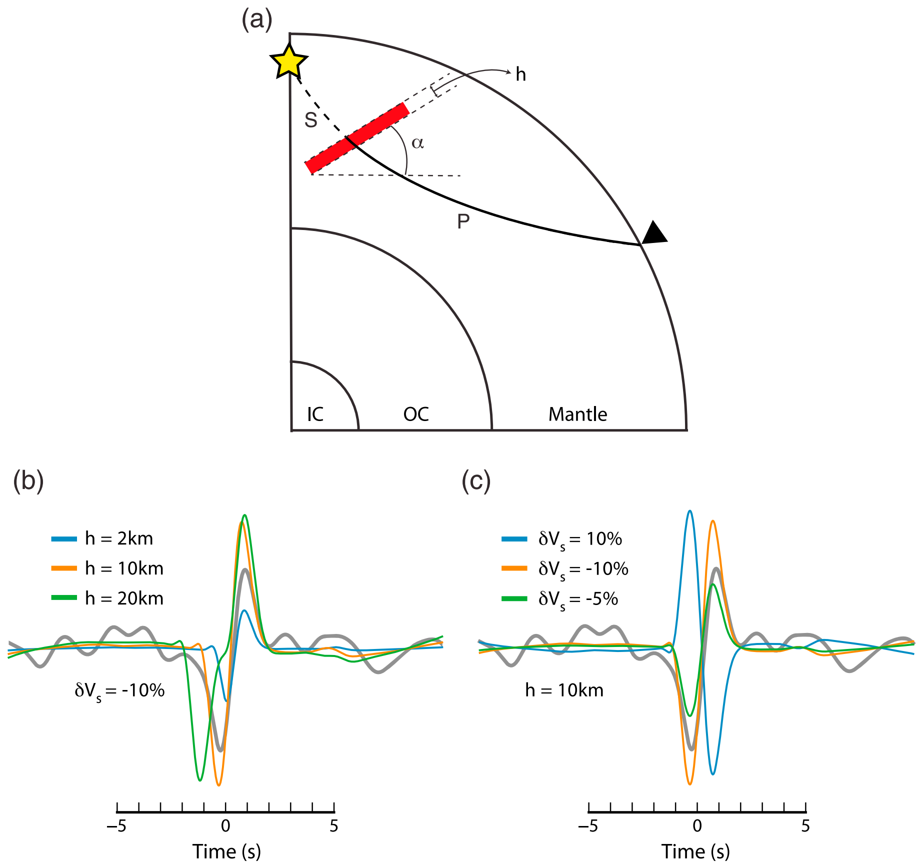

Figure 4. (a) Illustration of the model. The heterogeneity responsible for forming $S_{1750}P$ is modeled as a block at 1,750 km depth with a thickness h that makes an angle α with the equatorial plane. It has a velocity contrast δV_S with respect to the ambient mantle. (b) Synthetic waveforms for $h=2$ km, $h=10$ km, and $h=20$ km. $\delta V_S=-10\%$ in these simulations. (c) Synthetic waveforms for $\delta V_S=10\%$, $\delta V_S=-10\%$, and $\delta V_S=-5\%$. $h=10$ km in these simulations. For all simulations in Figures 4b and 4c, $\alpha=0°$, the epicentral distance is 65°, and the gray waveform is the stack of the recorded $S_{1750}P$ waveforms.

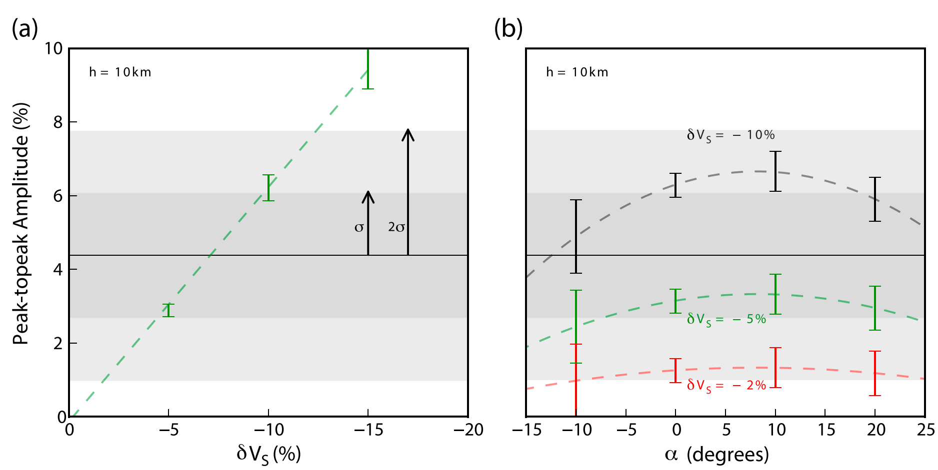

Figure 5. Peak-to-peak $S_{1750}P$ amplitude normalized to the radial *SV* component as a function of (a) δV_S and (b) block angle α. The horizontal black line indicates the mean value of the amplitude. Its two gray envelopes are one and two standard deviations wide. Vertical black bars are predicted amplitudes with error bars estimated from the minimum and maximum values for a range of epicentral distances.

4. Discussion and Conclusions

If small-scale heterogeneities that produce high-amplitude S_xP signals are indeed fragments of mid-ocean ridge basalt (MORB) subducted into the lower mantle, the analysis of S_xP waveforms can place important constraints on the elastic properties and composition of MORB at lower mantle conditions.

There is consensus that the density of MORB is 0.5% to 2% higher than the ambient mantle over the entire lower mantle range (e.g., Hirose et al., 1999; Irifune & Ringwood, 1987, 1993; Irifune & Tsuchiya, 2007; Litasov et al., 2004; Ricolleau et al., 2010). However, high-pressure experiments on the elastic properties of MORB are challenging and available estimates are based on ab initio modeling (e.g., Kawai & Tsuchiya, 2012; Kudo et al., 2012; Tsuchiya, 2011; Xu et al., 2008).

SiO_2 is an important component in MORB and undergoes a phase transition from stishovite to an orthorhombic $CaCl_2$ structure at midmantle conditions. Karki et al. (1997) first calculated from first principles the elastic parameters of stishovite and $CaCl_2$ and found a decrease in shear velocity. Tsuchiya et al. (2004) predicted that silica would exist in the $CaCl_2$ structure at 75 GPa along the geotherm of a subducting slab. If present in subducting slabs, silica will undergo this phase transition and produce seismic heterogeneities commonly observed near subduction zones.

Tsuchiya (2011) estimated that V_S is between 0 and 2% lower than the shear velocity of a pyrolitic mantle at a depth of 1,750 km due to a poststishovite transition. He found that V_P does not change appreciably. In constrast, Xu et al. (2008) did not include the effect of poststishovite and reported that V_S in a pyrolitic mantle increases with increasing basalt fraction. The presence of aluminum in silica further softens both stishovite and $CaCl_2$ (e.g., Bolfan-Casanova et al., 2009; Lakshtanov et al., 2007). Our observation occurs at 75 GPa at a temperature range of 1200–2000 K, well within the *P*-*T* conditions of $CaCl_2$ estimated by, for example, Nomura et al. (2010) and Ono et al. (2002).

The negative polarity of $S_{1750}P$ is a robust observation and implies that the heterogeneity that produces this arrival has a lower shear velocity than the ambient mantle. The mean amplitude of $S_{1750}P$ indicates that δV_S is between −1.6% and −12.4%. This estimate is uncertain because the recorded $S_{1750}P$ amplitude is highly variable and the modeling is influenced by the geometry and orientation of the heterogeneity. However, the lowest value (i.e., −1.6%) for our estimate of δV_S is consistent with the shear velocity reduction of MORB at deep-mantle pressures, estimated by Tsuchiya (2011) as shown in Figure 4. We therefore interpret $S_{1750}P$ as a *S* wave to *P* wave conversion by a small-scale, MORB fragment in a subducted slab in the lower mantle beneath the Brazil earthquake. The relatively low shear velocity of the MORB fragment is evidence for shear softening due to the postsitshovite phase transition in MORB in the deep mantle.

Seismological modeling of $S_{1750}P$ can benefit from additional broadband recordings to constrain waveform polarity and amplitude variability. In addition, estimates of the seismic properties of subducted MORB in the lower mantle will improve if we can consider the effects of off-azimuth wave propagation and *SH*-to-*P* wave conversions contributing to $S_{1750}P$. This requires computational resources that are currently not available to us.

Acknowledgments
This research was funded by the National Science Foundation under grant EAR–1644829. We acknowledge the University of Utah Center for High Performance Computing (CHPC) for computer resources and support. Michael S. Thorne was partially supported by NSF grant EAR–1401097. Seismic data have been provided by the Incorporated Research Institutions for Seismology (IRIS) and the Geological Survey of Canada. We thank Jennifer Jenkins and an anonymous reviewer for helpful comments. We thank Editor Noah Diffenbaugh for overseeing the editorial process.

References

Bolfan-Casanova, N., Andrault, D., Amiguet, E., & Guignot, N. (2009). Equation of state and post-stishovite transformation of Al-bearing silica up to 100 GPa and 3000 K. *Physics of the Earth and Planetary Interiors*, *174*(1), 70–77. https://doi.org/10.1016/j.pepi.2008.06.024

Castle, J. C., & van der Hilst, R. D. (2003). Searching for seismic scattering off mantle interfaces between 800 km and 2000 km depth. *Journal of Geophysical Research*, *108*(B2), 2095. https://doi.org/10.1029/2001JB000286

Fukao, Y., Widiyantoro, S., & Obayashi, M. (2001). Stagnant slabs in the upper and lower mantle transition region. *Reviews of Geophysics*, *39*(3), 291–323. https://doi.org/10.1029/1999RG000068

Grand, S. P., van der Hilst, R. D., & Widiyantoro, S. (1997). High resolution global tomography: A snapshot of convection in the Earth. *Geological Society of America Today*, *7*(4), 1–7.

Hirose, K., Fei, Y., Ma, Y., & Mao, H. K. (1999). The fate of subducted basaltic crust in the Earth's lower mantle. *Nature*, *397*(6714), 53–56. https://doi.org/10.1038/16225

Irifune, T., & Ringwood, A. E. (1987). Phase transformations in a harzburgite composition to 26 GPa: Implications for dynamical behaviour of the subducting slab. *Earth and Planetary Science Letters*, *86*(2–4), 365–376. https://doi.org/10.1016/0012-821X(87)90233-0

Irifune, T., & Ringwood, A. E. (1993). Phase transformations in subducted oceanic crust and buoyancy relationships at depths of 600–800 km in the mantle. *Earth and Planetary Science Letters*, *117*(1–2), 101–110. https://doi.org/10.1016/0012-821X(93)90120-X

Irifune, T., & Tsuchiya, T. (2007). Mineralogy of the Earth–Phase transitions and mineralogy of the lower mantle. *Treatise on Geophysics*, *2*, 33–62. https://doi.org/10.1029/2012JB009696

Jahnke, G., Thorne, M. S., Cochard, A., & Igel, H. (2008). Global *SH*-wave propagation using a parallel axisymmetric spherical finite-difference scheme: Application to whole mantle scattering. *Geophysical Journal International*, *173*(3), 815–826. https://doi.org/10.1111/j.1365-246X.2008.03744.x

Kaneshima, S. (2013). Lower mantle seismic scatterers below the subducting Tonga slab: Evidence for slab entrainment of transition zone materials. *Physics of the Earth and Planetary Interiors*, *222*, 35–46. https://doi.org/10.1016/j.pepi. 2013.07.001

Kaneshima, S. (2016). Seismic scatterers in the mid-lower mantle. *Physics of the Earth and Planetary Interiors*, *257*, 105–114. https://doi.org/10.1016/j.pepi.2016.05.004

Kaneshima, S., & Helffrich, G. (1998). Detection of lower mantle scatterers northeast of the Marianna subduction zone using short-period array data. *Journal of Geophysical Research*, *103*(B3), 4825–4838. https://doi.org/10.1029/97JB02565

Kaneshima, S., & Helffrich, G. (1999). Dipping low-velocity layer in the mid-lower mantle: Evidence for geochemical heterogeneity. *Science*, *283*(5409), 1888–1892. https://doi.org/10.1126/science.283.5409.1888

Kaneshima, S., & Helffrich, G. (2003). Subparallel dipping heterogeneities in the mid-lower mantle. *Journal of Geophysical Research*, *108*(B5), 2272. https://doi.org/10.1029/2001JB001596

Kaneshima, S., & Helffrich, G. (2010). Small scale heterogeneity in the mid-lower mantle beneath the circum-Pacific area. *Physics of the Earth and Planetary Interiors*, *183*(1), 91–103. https://doi.org/10.1016/j.pepi.2010.03.011

Karki, B. B., Stixrude, L., & Crain, J. (1997). Ab initio elasticity of three high-pressure polymorphs of silica. *Geophysical Research Letters*, *24*(24), 3269–3272. https://doi.org/10.1029/97GL53196

Kawai, K., & Tsuchiya, T. (2012). First principles investigations on the elasticity and phase stability of grossular garnet. *Journal of Geophysical Research*, *117*, B02202. https://doi.org/10.1029/2011JB008529

Kawakatsu, H., & Niu, F. (1994). Seismic evidence for a 920-km discontinuity in the mantle. *Nature*, *371*(6495), 301–305. https://doi.org/10.1038/371301a0

Kudo, Y., Hirose, K., Murakami, M., Asahara, Y., Ozawa, H., Ohishi, Y., & Hirao, N. (2012). Sound velocity measurements of $CaSiO_3$ perovskite to 133 GPa and implications for lowermost mantle seismic anomalies. *Earth and Planetary Science Letters*, *349*, 1–7. https://doi.org/10.1016/j.epsl.2012.06.040

Lakshtanov, D. L., Sinogeikin, S. V., Litasov, K. D., Prakapenka, V. B., Hellwig, H., Wang, J., & Li, J. (2007). The post-stishovite phase transition in hydrous alumina-bearing SiO_2 in the lower mantle of the Earth. *Proceedings of the National Academy of Sciences of the United States of America*, *104*(34), 13,588–13,590. https://doi.org/10.1073/pnas.0706113104

Li, J., & Yuen, D. A. (2014). Mid-mantle heterogeneities associated with Izanagi plate: Implications for regional mantle viscosity. *Earth and Planetary Science Letters*, *385*, 137–144. https://doi.org/10.1016/j.epsl.2013.10.042

Litasov, K., Ohtani, E., Suzuki, A., Kawazoe, T., & Funakoshi, K. (2004). Absence of density crossover between basalt and peridotite in the cold slabs passing through 660 km discontinuity. *Geophysical Research Letters*, *31*, L24607. https://doi.org/10.1029/2004GL021306

Niu, F. (2014). Distinct compositional thin layers at mid-mantle depths beneath northeast China revealed by the USArray. *Earth and Planetary Science Letters*, *402*, 305–312. https://doi.org/10.1016/j.epsl.2013.02.015

Niu, F., & Kawakatsu, H. (1997). Depth variation of the mid-mantle seismic discontinuity. *Geophysical Research Letters*, *24*(4), 429–432. https://doi.org/10.1029/97GL00216

Nomura, R., Hirose, K., Sata, N., & Ohishi, Y. (2010). Precise determination of post-stishovite phase transition boundary and implications for seismic heterogeneities in the mid-lower mantle. *Physics of the Earth and Planetary Interiors*, *183*(1), 104–109. https://doi.org/10.1016/j.pepi.2010.08.004

Ono, S., Hirose, K., Murakami, M., & Isshiki, M. (2002). Post-stishovite phase boundary in SiO_2 determined by in situ X-ray observations. *Earth and Planetary Science Letters*, *197*(3), 187–192. https://doi.org/10.1016/S0012-821X(02)00479-X

Ricolleau, A., Perrillat, J. P., Fiquet, G., Daniel, I., Matas, J., Addad, A., & Guignot, N. (2010). Phase relations and equation of state of a natural MORB: Implications for the density profile of subducted oceanic crust in the Earth's lower mantle. *Journal of Geophysical Research*, *115*, B08202. https://doi.org/10.1029/2009JB006709

Ritsema, J., Deuss, A. A., Van Heijst, H. J., & Woodhouse, J. H. (2011). S40RTS: A degree-40 shear-velocity model for the mantle from new Rayleigh wave dispersion, teleseismic traveltime and normal-mode splitting function measurements. *Geophysical Journal International*, *184*(3), 1223–1236. https://doi.org/10.1111/j.1365-246X.2010.04884.x

Shearer, P. M. (2007). *Deep Earth structure—Seismic scattering in the deep Earth, Treatise on Geophysics* (pp. 695–729). Amsterdam: Elsevier.

Thorne, M. S., Zhang, Y., & Ritsema, J. (2013). Evaluation of 1-D and 3-D seismic models of the Pacific lower mantle with *S*, SKS, and SKKS traveltimes and amplitudes. *Journal of Geophysical Research: Solid Earth*, *118*, 985–995. https://doi.org/10.1002/jgrb.50054

Tsuchiya, T. (2011). Elasticity of subducted basaltic crust at the lower mantle pressures: Insights on the nature of deep mantle heterogeneity. *Physics of the Earth and Planetary Interiors*, *188*(3), 142–149. https://doi.org/10.1016/j.pepi.2011.06.018

Tsuchiya, T., Caracas, R., & Tsuchiya, J. (2004). First principles determination of the phase boundaries of high-pressure polymorphs of silica. *Geophysical Research Letters*, *31*, L11610. http://doi.org/10.1029/2004GL019649

Vanacore, E., Niu, F., & Kawakatsu, H. (2006). Observations of the mid-mantle discontinuity beneath Indonesia from *S* to *P* converted waveforms. *Geophysical Research Letters*, *33*, L04302. https://doi.org/10.1029/2005GL025106

Vinnik, L., Niu, F., & Kawakatsu, H. (1998). Broadband converted phases from midmantle discontinuities. *Earth, Planets and Space*, *50*(11–12), 987–997. http://doi.org/10.1186/BF03352193

Xu, W., Lithgow-Bertelloni, C., Stixrude, L., & Ritsema, J. (2008). The effect of bulk composition and temperature on mantle seismic structure. *Earth and Planetary Science Letters*, *275*(1), 70–79. https://doi.org/10.1016/j.epsl.2008.08.012

Yang, Z., & He, X. (2015). Oceanic crust in the mid-mantle beneath west-central Pacific subduction zones: Evidence from *S* to *P* converted waveforms. *Geophysical Journal International*, *203*(1), 541–547. https://doi.org/10.1093/gji/ggv314